1995

Mathematical Modeling for the Discharge of a Metal Hydride Electrode

Pauline De Vidts
Texas A & M University - College Station

Javier Delgado

Ralph E. White
University of South Carolina - Columbia, white@cec.sc.edu

Publication Info

Published in *Journal of the Electrochemical Society*, Volume 142, Issue 12, 1995, pages 4006-4013.

De Vidts, P., Delgado, J., & White, R.E. (1995). Mathematical Modeling for the Discharge of a Metal-Hydride Electrode. *Journal of the Electrochemical Society*, *142*(12) 4006-4013.
Publisher's Version: http://dx.doi.org/10.1149/1.2048454

Mathematical Modeling for the Discharge of a Metal Hydride Electrode

Pauline De Vidts,* Javier Delgado, and Ralph E. White**

Department of Chemical Engineering, University of South Carolina, Columbia, South Carolina 29208, USA

ABSTRACT

A mathematical model for the discharge of a metal-hydride electrode was developed. The model was used to study the effect of various parameters on predicted discharge curves. The simulations obtained using the model show the expected decrease of charge utilization as the rate of discharge is increased. Increasing the particle size of the alloy and decreasing the diffusion coefficient of the hydrogen atoms in the hydride showed a similar effect on the discharge curves. The model simulations also show the critical role that the kinetic and transport parameters play in determining the overall shape of the predicted discharge curves for a metal-hydride electrode. The kinetic parameters used in the model predictions are those for $TiMn_{1.5}H_x$ ($x < 0.31$).

Introduction

The nickel/metal-hydride (NiOOH/MH) battery is replacing the nickel/cadmium battery in several of its applications. The NiOOH/MH cell has a discharge voltage comparable to that of the nickel/cadmium battery (1.2 V), higher energy density, and possibly longer cycle life. Currently, there is extensive research focused on the development of good metal-hydride (MH) electrodes to be used in NiOOH/MH batteries. Most of this research consists on the experimental testing of different alloys and electrode designs.[1-5] A mathematical model for a metal-hydride electrode can be useful to researchers and battery designers as a tool to investigate the effect on the electrode's behavior of various design parameters and operating conditions, saving resources that otherwise would be dedicated to costly and lengthy experiments.

Viitanen[6] developed a model for the discharge of a cylindrical metal-hydride electrode that includes the ohmic losses in the electrolyte and in the solid material, the charge-transfer reaction on the surface of the solid particles, and the diffusion of atomic hydrogen in the solid particles. However, this model does not include the mass transfer of electrolyte through the pores in the electrode and the electrolyte is treated as a dilute solution. Yang *et al.*[7,8] developed models for nonporous metal-hydride electrodes of different shapes: flat, cylindrical, and spherical.

Their models include the phenomena in the bulk and surface of the solid phase only. Similar models were presented by Conway and Wojtowicz[9] in which they evaluate the time-scales of hydrogen desorption assuming that the diffusion of hydrogen through the bulk of the alloy is the rate limiting step. These models[7-9] do not represent porous metal-hydride electrodes like those used in batteries.

The purpose of this paper is to present a mathematical model for the discharge of a porous metal-hydride electrode based on fundamental principles. The governing equations include the mass transfer in the electrolyte and in the solid metal-hydride particles, the ohmic losses in the electrolyte and in the solid phase, and a charge-transfer reaction is assumed to occur on the surface of the metal-hydride particles. Because the electrode is porous, the governing equations are derived using the volume averaging technique.[10] The electrolyte is an aqueous solution of KOH. The electrolyte concentrations used most commonly in practical applications falls between 6.0 to 7.1 M; thus, we treat the electrolyte as a concentrated solution. Also, in our model the properties of the electrolyte are a function of concentration.

The model predictions show that the controlling role of the various processes taking place in the electrode during discharge can depend on the operating conditions and electrode design. The diffusion of atomic hydrogen from the bulk of the MH particles to the surface of the particles becomes more limiting as the rate of discharge is increased and as the size of the MH particles is increased. Increasing the discharge current increases the rate of the charge-transfer reaction, and one observes that there is charge (hydrogen) left in the electrode at the end-of-discharge, meaning that the diffusion process is slow compared to the charge-transfer process. The mass transfer and ohmic drop in the electrolyte has little effect on the electrode potential

* Electrochemical Society Student Member.
** Electrochemical Society Active Member.

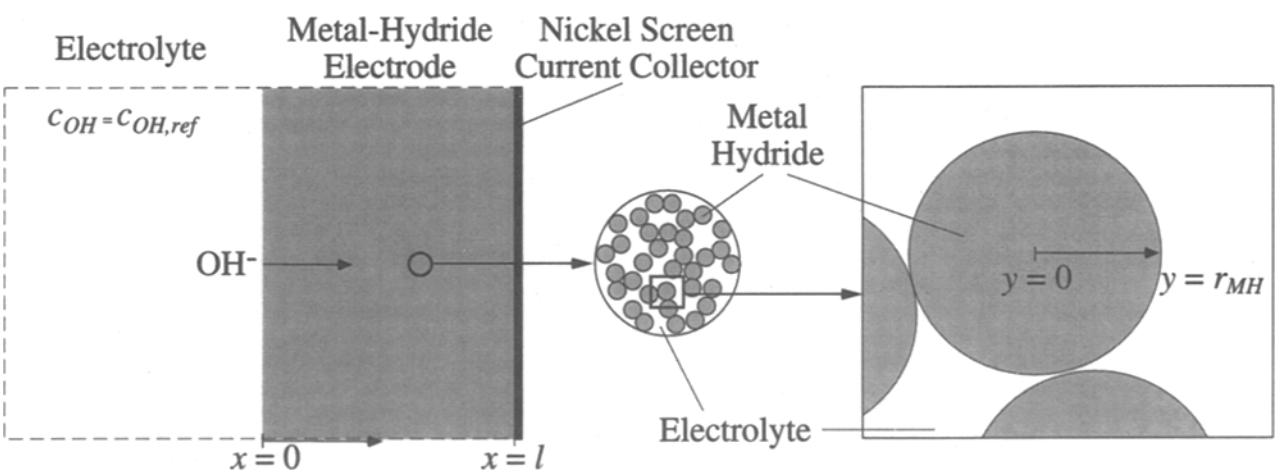

Fig. 1. Scheme of the model representation of the metal-hydride electrode. The surface of the electrode is exposed to a pool of electrolyte ($x = 0$). A current collector is located at the center of the electrode ($x = l$).

for thin electrodes. However, as the thickness of the electrode increases the potential drop in the electrolyte across the electrode increases rapidly. One should expect that this effect would become more important for an electrode operating in a cell or battery instead of being submerged in a pool of electrolyte as is the case for the electrode model presented here.

Model Development

Figure 1 presents a scheme of the metal-hydride (MH) electrode being modeled in this work. We assume that the MH electrode is immersed in a pool of electrolyte. The MH particles are assumed to consist of the metal-hydride material only, without any deposited metal layer on their surface. The metal-hydride electrode is a conducting porous material flooded with a concentrated KOH solution. Consequently, the model equations are derived using the volume-averaging technique for porous media[10] and Newman's theory for concentrated binary electrolytes.[11] We use a pseudo-two-dimensional approach to treat the mass transfer in the MH electrode in a similar way as we did in the model for a nickel hydroxide electrode.[12,13] In this pseudo-two-dimensional model, the x dimension is defined across the electrode and the pseudo-y dimension is defined inside the metal-hydride particles, as shown in Fig. 1. In our representation of the MH electrode the current collector (nickel screen) is placed in the center of the electrode, which corresponds to $x = l$. Thus, the total thickness of the MH electrode is $2l$. The surface of the electrode which is in contact with the pool of electrolyte corresponds to $x = 0$.

Electrode kinetics.—During discharge, the reaction at the MH electrode involves the oxidation of an adsorbed hydrogen to form water with a hydroxyl ion from the electrolyte. In this discharge model, we assume that the charge transfer takes place on the surface of the metal-hydride particles and does so according to a Volmer adsorption electrochemical reaction[14]

$$MH_{ads} + OH^- \xrightarrow{\text{discharge}} M + H_2O + e^- \quad [1]$$

The current density due to the reaction is assumed to be given by a Butler-Volmer expression

$$j = j_o \left\{ \exp\left[\frac{\alpha F}{RT}(\phi^{(s)} - \phi^{(l)} - U_{eq})\right] - \exp\left[\frac{-(1-\alpha)F}{RT}(\phi^{(s)} - \phi^{(l)} - U_{eq})\right]\right\} \quad [2]$$

in which $\phi^{(s)}$ is the potential in the solid phase, $\phi^{(l)}$ is the potential in the electrolyte, U_{eq} is the equilibrium potential of the reaction, α is the symmetry factor, and j_o is the exchange current density. The exchange current density and the equilibrium potential can be expressed in terms of their values at a given set of reference conditions

$$j_o = j_{o,ref}\left(\frac{a_H}{a_{H,ref}}\right)^{p(1-\alpha)}\left(\frac{a_{OH}}{a_{OH,ref}}\right)^{q(1-\alpha)}\left(\frac{a_{H_2O}}{a_{H_2O,ref}}\right)^{h\alpha} \quad [3]$$

$$U_{eq} = U_{eq,ref} - \frac{RT}{F}\ln\left(\frac{a_H}{a_{H,ref}}\right)^p - \frac{RT}{F}\ln\left(\frac{a_{OH}}{a_{OH,ref}}\right)^q + \frac{RT}{F}\ln\left(\frac{a_{H_2O}}{a_{H_2O,ref}}\right)^h \quad [4]$$

In Eq. 3 and 4, a_H, a_{OH}, and a_{H_2O} are the relative activities of adsorbed hydrogen, OH^- ions, and water, respectively. The exponents p, q, and h are the orders of reaction of the various reacting species. The reference conditions are denoted by the subscript ref.

Substituting Eq. 3 and 4 into Eq. 2, we obtain an expression for the current density in terms of the reference conditions

$$j = j_{o,ref}\left\{\left(\frac{a_H}{a_{H,ref}}\right)^p\left(\frac{a_{OH}}{a_{OH,ref}}\right)^q \exp\left[\frac{\alpha F}{RT}(\phi^{(s)} - \phi^{(l)} - U_{eq,ref})\right] - \left(\frac{a_{H_2O}}{a_{H_2O,ref}}\right)^h \exp\left[\frac{-(1-\alpha)F}{RT}(\phi^{(s)} - \phi^{(l)} - U_{eq,ref})\right]\right\} \quad [5]$$

The relative activity of adsorbed hydrogen, a_H, is defined as

$$a_H = \frac{f_H c_H}{\lambda_M^\circ} \quad [6]$$

in which c_H is the concentration of hydrogen atoms in the solid phase in moles per unit of volume of solid, f_H is the molar activity coefficient of the hydrogen atom in the MH electrode, and λ_M° is the absolute activity of pure metal M in the absence of hydrogen ($\lambda_M^\circ = 1$). We assume that f_H is equal to one.

If we express the relative activities a_H, a_{OH}, and a_{H_2O} in terms of concentrations and assume that the relative activity of water is constant and equal to that at the reference conditions, Eq. 5 becomes

$$j = j_{o,ref}\left\{\left(\frac{c_H}{c_{H,ref}}\right)^p\left(\frac{c_{OH}}{c_{OH,ref}}\right)^q \exp\left[\frac{\alpha F}{RT}(\phi^{(s)} - \phi^{(l)} - U_{eq,ref})\right] - \exp\left[\frac{-(1-\alpha)F}{RT}(\phi^{(s)} - \phi^{(l)} - U_{eq,ref})\right]\right\} \quad [7]$$

If we measure $U_{eq,ref}$ with respect to a Hg/HgO reference electrode which is at conditions denoted by the subscript RE, we have

$$U_{eq,ref} = U^\theta - U_{RE}^\theta - \frac{RT}{F}\ln a_{H,ref}^p - \frac{RT}{F}\ln\left(\frac{a_{OH,ref}^q}{a_{OH,RE}}\right) - \frac{RT}{F}\ln\left(\frac{a_{H_2O,ref}^h}{a_{H_2O,RE}^{1/2}}\right) \quad [8]$$

In arriving at Eq. 8, we have assumed that the orders of reaction for the reactants in the Hg/HgO electrode reaction ($1/2\ HgO + 1/2\ H_2O + e^- \rightleftarrows 1/2\ Hg + OH^-$) are given by their stoichiometric coefficients. Assuming that the Hg/HgO reference electrode is at the reference conditions used in Eq. 4, that is $a_{OH,RE} = a_{OH,ref}$ and $a_{H_2O,RE} = a_{H_2O,ref}$, Eq. 8 becomes

$$U_{eq,ref} = U^\theta - U_{RE}^\theta - \frac{RT}{F}\ln a_{H,ref}^p - \frac{RT}{F}\ln\left(a_{OH,ref}^{q-1}\right) - \frac{RT}{F}\ln\left(a_{H_2O,ref}^{h-1/2}\right) \quad [9]$$

Further, if we assume that $a_{H_2O,ref} = 1$ and $q = 1$, we obtain

$$U_{eq,ref} = U^\theta - U_{RE}^\theta - \frac{RT}{F}\ln a_{H,ref}^p \quad [10]$$

Substituting the relative activity of atomic hydrogen by Eq. 6 with $f_H = 1$, the equilibrium potential at reference conditions becomes

$$U_{eq,ref} = U^\theta - U_{RE}^\theta - \frac{RT}{F}\ln c_{H,ref}^p \quad [11]$$

with $U^\theta = -0.828$ V and $U_{RE}^\theta = 0.0983$ V.

Yayama *et al.*[15] used a similar kinetic expression to study the metal hydride $TiMn_{1.5}H_x$ ($x < 0.31$). They obtained values for the kinetic parameters (p, α, and $j_{o,ref}$) which are used in the simulations presented in this paper.

Governing equations.—The governing equations are written for four dependent variables in the x direction and one in the y direction. The dependent variables in the x direction are: concentration of electrolyte, c_{OH}; current density in the electrolyte, $i^{(l)}$; potential in the electrolyte, $\phi^{(l)}$; and, potential in the solid phase, $\phi^{(s)}$. The dependent variable in the y direction is the concentration of atomic hydrogen in the MH particles, c_H.

Equations in the x direction.—Material balance of electrolyte.—The electrolyte concentration inside the electrode changes with time and position because of the electrochemical reaction and mass transfer

$$\epsilon\frac{\partial c_{OH}}{\partial t} = \epsilon^\gamma\left(\frac{\partial D_{KOH}}{\partial x}\frac{\partial c_{OH}}{\partial x} + D_{KOH}\frac{\partial^2 c_{OH}}{\partial x^2}\right) + \frac{t_-^\star}{F}\frac{\partial i^{(l)}}{\partial x} - \frac{a_{MH}}{F}j \quad [12]$$

Table I. Parameter values used in the simulations.

Parameter	Value	Parameter	Value
α	0.23	ϵ	0.30
p	0.67	a_{MH} [b]	2100 cm^2/cm^3
q	1.0	Q_{MH}	16.8×10^{-3} Ah/cm^2
$j_{o,ref}$	2.84×10^{-4} A/cm^2	l	0.04 cm
D_H	5×10^{-11} cm^2/s	γ	1.5
$c_{H,ref}$ [a]	22.41×10^{-3} mol/cm^3	i_{cell} (C/10 rate)	-1.68×10^{-3} A/cm^2
$\sigma_{MH}^{(s)}$	41505.1 S/cm	$c_{OH,ref}$	6.0×10^{-3} mol/cm^3
r_{MH}	10^{-3} cm	T	298.15 K
$\phi_o^{(l)}$	0.47 V (arbitrary)		

[a] Maximum hydrogen concentration.
[b] Calculated using Eq. 27.

where ϵ is the porosity of the electrode, D_{KOH} is the diffusion coefficient of free electrolyte, $t_-^\star$ is the transference number of the OH^- ions relative to the molar average velocity of the solution, and a_{MH} is the electroactive surface area of the metal-hydride particles that is in contact with the electrolyte per unit volume of electrode.

Researchers have observed changes in volume of the MH material between 15 to 27% during charge/discharge cycles of MH electrodes.[3,5,16] The changes in volume are larger for MH materials that absorb larger amounts of hydrogen. This change in volume usually causes the pulverization of the MH material with particle size reductions from 100 μm to as low as 6 μm in diameter.[5] This may lead to a change in the porosity of the electrode during its operation. During the precycling of the electrode (activation) the MH material is pulverized to some degree. As a first approach, we assume that this pulverization affects the particle size only, not the porosity of the electrode. And we assume that during the operation of the electrode there is no variation in particle size nor in porosity. Thus, in this analysis we assume that the porosity is constant and its value is that reported by Yayama[15] for a $TiMn_{1.5}H_x$ electrode. Yayama built the $TiMn_{1.5}H_x$ electrode with particles of 20 to 50 μm in diam. We choose a value of 20 μm as the average particle diameter after the precycling of the electrode (activation). For materials that absorb large amounts of hydrogen the assumption of constant porosity and particle size may have to be lifted.

Modified Ohm's law for the liquid phase.—The current density at a given position in the electrolyte inside the electrode results from a gradient in the electrolyte's electric potential and a gradient in electrolyte concentration. Using a Hg/HgO reference electrode to measure the potential in the liquid phase, we have

$$\frac{-i^{(l)}}{\epsilon^\gamma \kappa} = \frac{\partial \phi^{(l)}}{\partial x} + \frac{2RT}{F}\left(1 + \frac{d \ln f_\pm}{d \ln c_{OH}}\right)\left[1 - \left(1 + \frac{2c_{OH}}{c_{H_2O}}\right) t_-^\star + \frac{3c_{OH}}{2c_{H_2O}}\right] \frac{\partial \ln c_{OH}}{\partial x} \quad [13]$$

in which κ is the specific conductivity of free electrolyte, c_{H_2O} is the concentration of water, and $f_\pm$ is the mean molar activity coefficient of the KOH electrolyte.

Transfer current per unit volume.—The gradient in the x direction of the current density in the electrolyte is equal to the current density due to the electrochemical reaction multiplied by the electroactive surface area per unit of volume of electrode

$$\frac{\partial i^{(l)}}{\partial x} = a_{MH} j \quad [14]$$

Conservation of charge.—The current density in the cell is equal to the sum of the current in the liquid phase and solid phase

$$i^{(l)} - \sigma_{MH}^{(s)}(1 - \epsilon)\frac{\partial \phi^{(s)}}{\partial x} = i_{cell} \quad [15]$$

in which $\sigma_{MH}^{(s)}$ is the specific conductivity of the MH electrode material and i_{cell} is the current density applied to the electrode.

Boundary conditions at the electrode/electrolyte interface ($x = 0$)

$$c_{OH}|_{x=0} = c_{OH,ref} \quad [16]$$

$$i^{(l)}|_{x=0} = i_{cell} \quad [17]$$

$$\phi^{(l)}|_{x=0} = \phi_o^{(l)} \quad [18]$$

$$\left.\frac{\partial i^{(l)}}{\partial x}\right|_{x=0} = a_{MH} j \quad [19]$$

Equation 16 indicates that the concentration of electrolyte at the surface of the electrode is kept at a constant value, which is chosen to be the reference concentration. The current density in the electrolyte is assumed to be equal to the applied current as represented by Eq. 17. The potential in the electrolyte is set to an arbitrary value $\phi_0^{(l)}$. The boundary condition for the potential in the solid phase is given by Eq. 19, which indicates that the gradient in the x direction of the current density in the electrolyte is equal to the charge being transferred per unit volume from the electrolyte to the solid phase in the electrode due to the electrochemical reaction.

Boundary conditions at the center of the metal-hydride electrode ($x = l$)

$$\left.\frac{\partial c_{OH}}{\partial x}\right|_{x=l} = 0 \quad [20]$$

$$\frac{-i^{(l)}}{\epsilon^\gamma \kappa} = \frac{\partial \phi^{(l)}}{\partial x} + \frac{2RT}{F}\left(1 + \frac{d \ln f_\pm}{d \ln c_{OH}}\right)\left[1 - \left(1 + \frac{2c_{OH}}{c_{H_2O}}\right) t_-^\star + \frac{3c_{OH}}{2c_{H_2O}}\right] \frac{\partial \ln c_{OH}}{\partial x} \quad [21]$$

$$\frac{\partial i^{(l)}}{\partial x} = a_{MH} j \quad [22]$$

$$i^{(l)} - \sigma_{MH}^{(s)}(1 - \epsilon)\frac{\partial \phi^{(s)}}{\partial x} = i_{cell} \quad [23]$$

Equations in the y direction.—The diffusing species in the solid phase of the MH electrode is atomic hydrogen (H). Assuming that there are no gradients in the angular directions inside and on the surface of the spherical particles, the diffusion equation applied to the atomic hydrogen in the metal hydride is

$$\frac{\partial c_H}{\partial t} = D_H\left(\frac{\partial^2 c_H}{\partial y^2} + \frac{2}{y}\frac{\partial c_H}{\partial y}\right) \quad [24]$$

where y is the coordinate for the pseudo-second dimension (see Fig. 1).

At the surface of the solid particles the atomic hydrogen in the metal-hydride reacts electrochemically with the electrolyte according to reaction 1. Thus, the flux of hydrogen is equal to the reaction rate in which H participates

$$-D_H \left.\frac{\partial c_H}{\partial y}\right|_{y=r_{MH}} = \frac{i}{F} \quad [25]$$

At the center of the solid particles the flux of atomic hydrogen is equal to zero

$$-D_H \left.\frac{\partial c_H}{\partial y}\right|_{y=0} = 0 \quad [26]$$

Table II. Properties of the electrolyte at 298.15 K.

Diffusion coefficient

$$D_{KOH} = \overline{D}_{KOH}\left(1.0 - 4.0804\, c_{OH}^{1/2} + 286.2\, c_{OH} - 3809.7\, c_{OH}^{3/2} + 14415.0\, c_{OH}^{2}\right)$$

$$\overline{D}_{KOH} = \exp\left(-10.467 - 8.1607\, c_{OH}^{1/2} + 286.2\, c_{OH} - 2539.8\, c_{OH}^{3/2} + 7207.5\, c_{OH}^{2}\right)$$

Specific conductivity

$$\kappa = c_{OH} \exp\left(5.5657 - 6.1538\, c_{OH}^{1/2} + 13.408\, c_{OH} - 1075.8\, c_{OH}^{3/2}\right)$$

Ratio of electrolyte to water concentration

$$\frac{c_{OH}}{c_{H_2O}} = \exp\left(-6.8818 + 118.75\, c_{OH}^{1/2} - 1030.5\, c_{OH} + 4004.7\, c_{OH}^{3/2}\right)$$

Mean molar activity coefficient of the electrolyte

$$f_{\pm} = \gamma_{\pm}\left(\frac{\rho_{H_2O}}{\rho - M_{KOH} c_{OH}}\right)$$

with

$$\ln \gamma_{\pm} = \frac{-1.1813\sqrt{m}}{1+\sqrt{m}} + 0.3848\, m - 0.03205\, m^{3/2}$$

$$\rho = 1.0002 + 45.726\, c_{OH} - 601.63\, c_{OH}^{2}$$

$$m = \frac{1000\, c_{OH}}{\rho - M_{KOH} c_{OH}}$$

The transfer number: $t^{\star} = 0.78$

The model was solved using the parameter values and operating conditions given in Tables I and II. The kinetic parameters are those reported by Yayama *et al.*[15] for $TiMn_{1.5}H_x$. Lacking the true value of the diffusion coefficient of atomic hydrogen in $TiMn_{1.5}$, we assume a value of the order of magnitude of that for Inconel,[17] that is 5×10^{-11} cm^2/s. Ciureanu *et al.*[18] estimated the diffusion coefficient of H in $Ni_{64}Zr_{36}$ to be approximately 4×10^{-11} cm^2/s. It has to be noted that the diffusion coefficient may be as high as that of $LaNi_5$ which has been reported to be approximately 3×10^{-8} cm^2/s.[19,20] The conductivity of the alloy, $\sigma_{MH}^{(s)}$ was estimated using the rule of mixtures on the conductivity of the pure materials (Ti and Mn). The active surface area, a_{MH}, was estimated assuming that the spherical alloy particles are all of the same size and their entire surface is exposed to the electrolyte, leading to the following expression

$$a_{MH} = \frac{3(1-\epsilon)}{r_{MH}} \qquad [27]$$

The properties D_{KOH}, κ, and c_{OH}/c_{H_2O} are functions of the electrolyte concentration, c_{OH}. We obtained correlations for these properties by fitting polynomials of $c_{OH}^{1/2}$ to the logarithm of each property. The data for these correlations were taken from Lobo[21] and Lobo and Quaresma[22]; the resulting expressions are presented in Table II.

To solve the system of equations we used finite difference approximations for the spatial derivatives and solved the resulting system of ordinary differential equations over time with DASSL.[23] The initial conditions are listed in Table III.

Results

The discharge curves presented below are plotted against the state of discharge of the electrode (*SOD*). The state of discharge is defined as

Table III. Initial conditions used in the simulations.

Variable	Value
c_{OH}	6.0×10^{-3} mol/cm^3
$i^{(l)}$	0
$\phi^{(l)}$	$\phi_o^{(l)}$
$\phi^{(s)}$	$U_{eq,ref} + \phi^{(l)}$
c_H	22.41×10^{-3} mol/cm^3

$$SOD = \frac{-i_{cell} t}{Q_{MH}} \qquad [28]$$

in which t is the time elapsed from the beginning of discharge and Q_{MH} is the theoretical maximum charge per unit of projected electrode area of the MH electrode. The electrode potential shown in the plots is defined as the difference between the potential in the alloy at $x = l$ (position of the current collector) and the potential in the electrolyte at $x = 0$

$$\text{Electrode potential} = \phi^{(s)}|_{x=l} - \phi^{(l)}|_{x=0} \qquad [29]$$

Figure 2 shows curves of discharge potentials *vs.* the state of discharge at various discharge rates. We can see that as the discharge rate increases the state of discharge at the end-of-discharge decreases. This behavior is explained by the depletion of atomic hydrogen on the surface of the MH particles at high discharge rates, because the hydrogen diffusion from the bulk of the hydride is slow compared to the rate of the electrochemical reaction occurring on the surface of the particles. This causes the potential to drop before all the hydrogen contained in the particles has been reacted, because the concentration of hydrogen on the surface of the particles is close to zero. Thus, there is charge left in the electrode (hydrogen) at the end-of-discharge. To illustrate this process, Fig. 3 and 4 show the concentration of hydrogen inside the metal-hydride for two rates of discharge, $C/2$ and $C/10$, respectively. In both cases, the hydrogen concentration decreases toward the solid/electrolyte interface ($y = 0.001$ cm) where the hydrogen is being consumed by the charge-transfer reaction. As the discharge proceeds the overall hydrogen concentration decreases in the solid. At the end-of-discharge (cutoff voltage of -0.5 V) the hydrogen concentration on the solid/electrolyte interface reaches a value close to zero which causes the potential of the electrode to change rapidly to more positive values. In Fig. 3, one can see from the hydrogen concentration distribution at the end-of-discharge ($t = 1.62$ h) that there is still a considerable amount of hydrogen left in the electrode; approximately 20% of the maximum hydrogen content. However, for a lower rate of discharge the amount of hydrogen left in the electrode at the end-of-discharge is much smaller (approximately 5% of the maximum hydrogen content), as shown in Fig. 4.

In Fig. 5 we can see that increasing the particle size or reducing the value of the atomic hydrogen diffusion coefficient affects the electrode behavior in the same way as increasing the discharge rate, because this also makes the diffusion process slow compared to the charge-transfer reaction. Thus, the surface concentration of hydrogen drops prematurely at a given discharge rate, and we observe the steep potential drop before all the charge has been used. From Fig. 5, we can see that for $D_H = 5 \times 10^{-11}$ cm^2/s a

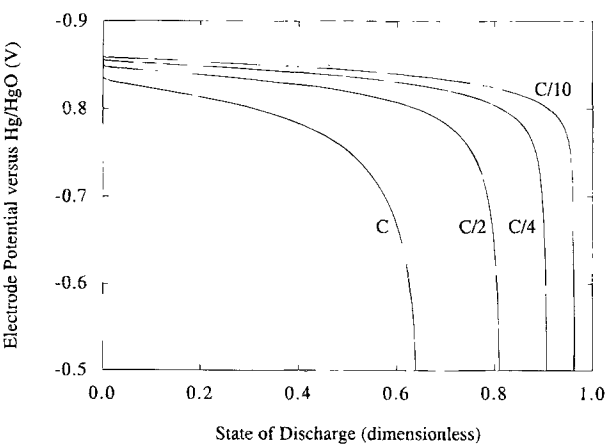

Fig. 2. Predicted electrode potential for various rates of discharge (*C* rate = -16.8×10^{-3} A/cm^2). The state of discharge and the electrode potential are defined in Eq. 28 and 29, respectively.

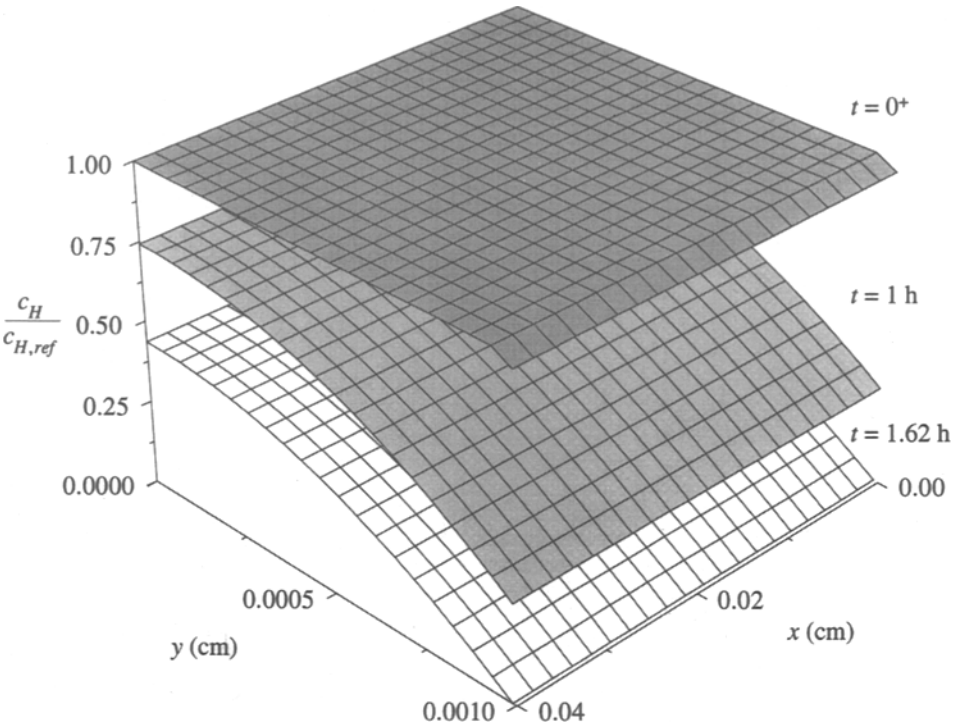

Fig. 3. Predicted hydrogen concentration distribution inside the metal-hydride material across the electrode for a discharge rate of C/2 ($i_{cell} = -8.4 \times 10^{-3}$ A/cm^2).

particle size of approximately 14 μm of diameter corresponds to the curve for $D_H/r_{MH}^2 = 10^{-4}$ s^{-1}, which results on a fully discharged electrode by the end of discharge (state of discharge equals one). Thus, for $D_H = 5 \times 10^{-11}$ cm^2/s a particle size of 14 μm or less will eliminate the controlling effect of the hydrogen diffusion process on the discharge behavior. However, if the diffusion coefficient is of the order of magnitude of that for $LaNi_5$, 3×10^{-8} cm^2/s, the particle size could be as large as 340 μm in diameter without making the diffusion process have a controlling effect on the discharge behavior. This means that if the diffusion coefficient is of the order of magnitude of 10^{-8} the diffusion process would not have a controlling effect in typical MH electrodes because usually the initial particle size is not larger than 100 to 70 μm. However, if the diffusion coefficient is approximately 5×10^{-11} cm^2/s, the diffusion process is expected to have a controlling role on the discharge behavior because the particle size in practical electrodes may easily exceed 14 μm, despite the pulverization caused by cycling of the electrode.

The controlling role that the hydrogen diffusion process may have on the electrode's behavior, as opposed to that of the reactions taking place on the hydride surface, is an important factor to consider in determining the kinetic parameters of a MH electrode because the performance of the electrode may be in mixed control (*i.e.*, not kinetically controlled nor diffusion controlled alone).

Figures 6 and 7 show the effect of kinetic parameters on the model simulations. Figure 6 shows that smaller values of p produce electrode potential curves with less overpotential, which is attractive for battery electrodes. In Fig. 7 we see that the larger the exchange current density is (evaluated at reference conditions) the smaller is the resulting electrode overpotential. The value of the parameter p reflects the dependence of the exchange current density on the hydrogen concentration in the alloy. From Eq. 3 we see that the smaller the value of p, the less dependent is the exchange current density on the hydrogen concentration. Therefore, if we were comparing MH electrodes made with different MH materials, those of materials with a small value of p and large $j_{o,ref}$ would be the most attractive for battery electrodes.

Figure 8 shows the effect of the electrode thickness on the potential drop in the electrolyte. The potential drop in the electrolyte across the electrode is defined as

$$\text{Potential drop in the electrolyte} = \phi^{(l)}|_{x=l} - \phi^{(l)}|_{x=0} \quad [30]$$

The values for l shown in Fig. 8 correspond to the half thickness of the electrode. As expected, the potential drop in the electrolyte increases as the thickness of the electrode increases, because the ohmic resistance increases. We can see that this drop is very small (~2 mV) for an $l = 0.04$ cm compared to the electrode overpotential of about 10 mV (from the curve at $C/2$ in Fig. 2). However, this drop increases rapidly as the electrode thickness increases, reaching values between 20 to 30 mV for $l = 0.16$ cm. Note that the curve for $l = 0.16$ cm has a negative slope with respect to the state of discharge. The reason for this slope is that during discharge there is a distribution of OH^- (electrolyte) species that is developed inside the electrode, because OH^- is consumed by the electrochemical reaction and is replenished through diffusion from the surface of the electrode. The diffusion path for OH^- becomes longer for thicker electrodes, and thus, the OH^- ions are replenished at a lower rate relative to their consumption by the electrochemical reaction, leading to a decrease in the concentration of OH^- toward the center of the electrode. A lower concentration of electrolyte results in lower electrolyte conductivity; consequently, the potential drop in the electrolyte is larger. The effect of ohmic resistance and mass transfer in the electrolyte may become much more important in an electrode operating in a cell or battery instead of a pool of electrolyte. In a cell, there is not an infinite supply of OH^- at the surface of the electrode as we have assumed here; thus, the electrolyte concentration may decrease more sharply during discharge in a battery than in the experimental system that was modeled here.

Conclusions

A mathematical model for the discharge of a metal hydride electrode was developed. The model was used to study the effect of various parameters on predicted discharge curves. The simulations obtained using the model show the expected decrease on charge utilization as the rate of discharge is increased. As the reaction rate is increased through increasing the discharge current there is charge (hydrogen) left in the electrode at the end-of-discharge, meaning that the diffusion process is slow compared to the charge-transfer process. The same electrode

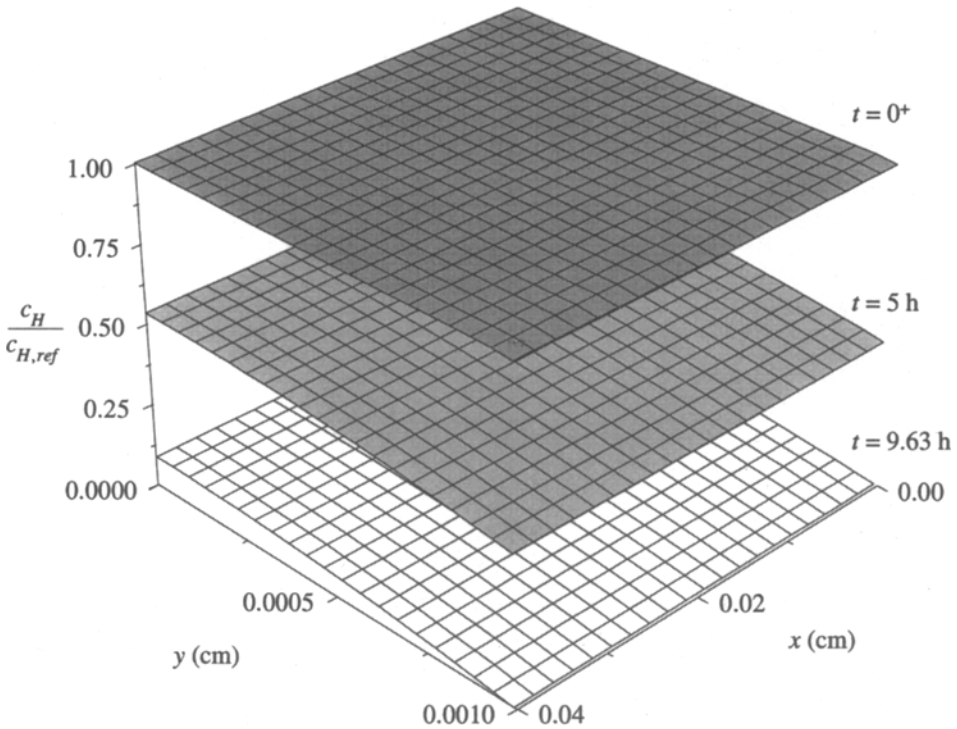

Fig. 4. Predicted hydrogen concentration distribution inside the metal-hydride material across the electrode for a discharge rate of C/10 ($i_{cell} = -1.68 \times 10^{-3}$ A/cm^2).

behavior is obtained by increasing the particle size or decreasing the hydrogen diffusion coefficient because by doing this we are making the diffusion process slow relative to the charge-transfer reaction on the surface of the particles.

The dependence of the exchange current density upon the state of discharge (atomic hydrogen concentration) may be a good indicator of the quality of the hydride material as an electrode. The best MH materials would be those with the highest exchange current density at any given conditions and the smallest dependence of the exchange current density on the hydrogen content in the electrode; that is, the reaction order p (see Eq. 3).

The mass transfer and ohmic drop in the electrolyte can become important for thick electrodes. Also, this effect may be more severe for electrodes operating in a battery instead of a pool of electrolyte, because the surface of the MH electrode would not be exposed to an infinite supply of OH^- ions (electrolyte) as we have assumed in the model presented here.

In this work we have assumed that the porosity of the electrode and particle size are constant during the operation of the electrode. This assumption may have to be lifted for materials that absorb large amounts of hydrogen because they may exhibit large variations in particle size and porosity. Also, the model presented here is limited to electrodes manufactured with MH particles that have not been covered with some metal layer (for example copper). Several researchers have shown that electrodes made with coated MH particles have longer cycle life and better charge/discharge characteristics.[3,5,24] The model presented here can be made more general by including a layer of coating on the MH particles, which will be considered in future work.

Battery designers and researchers can use the model presented here as a tool to help study the performance of metal-hydride electrodes. For example, upon measuring the kinetic parameters of a given metal-hydride material, the mathematical model can be used to predict the behavior of an electrode made of such a material, saving resources that otherwise would be dedicated to costly and lengthy experiments. Also, the researcher or battery designer can use the model to study the effect of the design

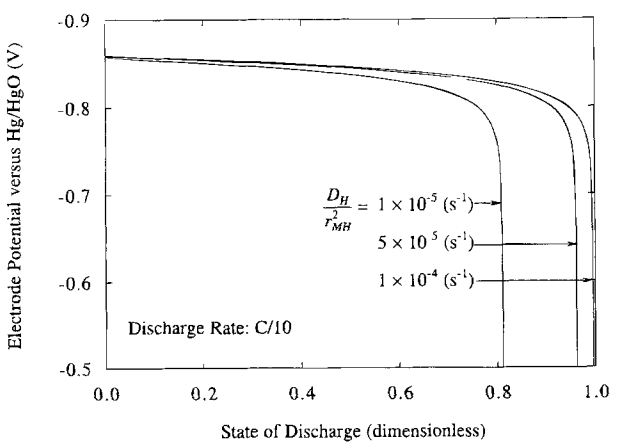

Fig. 5. Predicted electrode potential for various values of the ratio between the hydrogen diffusion coefficient and the metal-hydride particle radius. The state of discharge and the electrode potential are defined in Eq. 28 and 29, respectively.

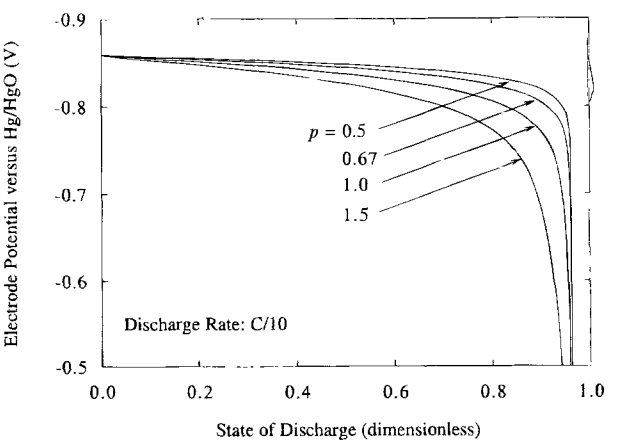

Fig. 6. Predicted electrode potential for various values of the order of reaction of hydrogen (p). The state of discharge and the electrode potential are defined in Eq. 28 and 29, respectively.

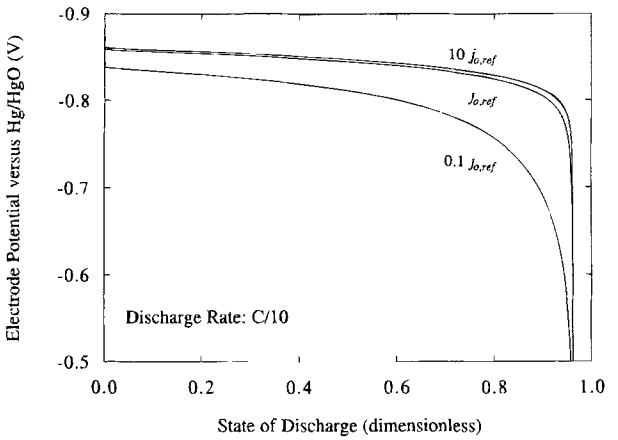

Fig. 7. Predicted electrode potential for various values of the exchange current density at reference conditions. The state of discharge and the electrode potential are defined in Eq. 28 and 29, respectively.

parameters and operating conditions on the electrode's behavior.

Acknowledgments

The authors acknowledge the financial support from the Department of Energy, the Office of Research and Development of the United States Central Intelligence Agency, and the NASA Center for Space Power at Texas A&M University.

Manuscript submitted April 5, 1995; revised manuscript received July 6, 1995.

The University of South Carolina assisted in meeting the publication costs of this article.

LIST OF SYMBOLS

a_H	relative activity of adsorbed hydrogen
$a_{H,ref}$	relative activity of adsorbed hydrogen at reference conditions
a_{OH}	relative activity of OH^-
$a_{OH,ref}$	relative activity of OH^- at reference conditions
a_{H_2O}	relative activity of water
$a_{H_2O,ref}$	relative activity of water at reference conditions
a_{MH}	electroactive surface area per unit volume of metal-hydride electrode, cm^2/cm^3
c_H	concentration of atomic hydrogen in the metal-hydride particles, mol/cm^3 of alloy
$c_{H,ref}$	reference concentration of atomic hydrogen, mol/cm^3 of alloy
c_{OH}	concentration of electrolyte, mol/cm^3
$c_{OH,ref}$	reference concentration of electrolyte, mol/cm^3
c_{H_2O}	concentration of water, mol/cm^3
D_{OH}	diffusion coefficient of the electrolyte, cm^2/s

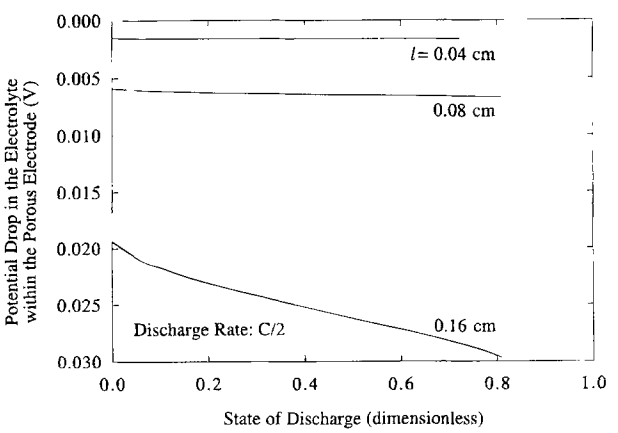

Fig. 8. Predicted potential drop in the electrolyte across the electrode for various thicknesses of the electrode. The state of discharge and the potential drop in the electrolyte are defined in Eq. 28 and 30, respectively.

$\overline{D}_{OH}$	integral diffusion coefficient of the electrolyte, cm^2/s
D_H	diffusion coefficient of atomic hydrogen in the metal-hydride particles, cm^2/s
F	Faraday's constant, 96,487 C/eq
$f_\pm$	mean molar activity coefficient of the electrolyte
h	order of reaction for water
H_{ads}	adsorbed H atom on the surface of the metal-hydride material
i_{cell}	current density applied to the cell, A/cm^2 of electrode
$i^{(l)}$	current density in the electrolyte, A/cm^2
j	current density due to the electrochemical reaction, A/cm^2 of active surface area
j_o	exchange current density of the electrochemical reaction, A/cm^2 of active surface area
$j_{o,ref}$	exchange current density of the electrochemical reaction evaluated at reference conditions, A/cm^2 of active surface area
l	half thickness of the metal-hydride electrode, cm
M	metal site
m	molality of the electrolyte solution, mol/kg
p	order of reaction for the atomic hydrogen
q	order of reaction for hydroxyl ions
Q_{MH}	theoretical maximum charge of the metal-hydride electrode, C/cm^2 of electrode
r_{MH}	radius of the metal-hydride particles, cm
R	universal gas constant, 8.314 J/mol K
SOD	state of discharge of the electrode at time t, defined as $SOD = -i_{cell}t/Q_{MH}$
t	time, s
T	temperature, K
$t_-^\star$	transference number of the electrolyte with respect to the average molar velocity
$U_{eq,ref}$	equilibrium potential of reaction 1 evaluated at the reference concentrations, V
U^θ	standard potential of reaction 1, V
U_{RE}^θ	standard potential of reference electrode reaction, V
x	spatial coordinate across the electrode, cm
y	coordinate for the pseudo-second dimension defined in the metal-hydride particles, cm

Greek

α	symmetry factor in the anodic direction
ϵ	porosity of the metal-hydride electrode
$\phi^{(l)}$	electric potential in the electrolyte, V
$\phi_o^{(l)}$	arbitrary value for the potential in the electrolyte at $x = 0$, V
$\phi^{(s)}$	electric potential in the solid phase, V
$\gamma_\pm$	mean activity coefficient of the electrolyte in molal basis
κ	specific conductivity of the electrolyte, S/cm
λ_M°	absolute activity of the pure metal M
ρ	density of the electrolyte solution, g/cm^3
ρ_{H_2O}	density of pure water, g/cm^3
$\sigma_{MH}^{(s)}$	specific conductivity of the metal-hydride, S/cm

REFERENCES

1. K. Petrov, A. A. Rostami, A. Visintin, and S. Srinivasan, *This Journal,* **141,** 1747 (1994).
2. Y. Sakamoto, K. Kuruma, S. Hirano, and M. Hirata, *ibid.,* **141,** 1740 (1994).
3. B. V. Ratnakumar, B. Otzinger, S. Di Stefano, and G. Halpert, JPL D-11161, Jet Propulsion Laboratory, California Institute of Technology, Pasadena, CA (1993).
4. M. A. Fetcenko, S. Venkatesan, and S. R. Ovshinsky, in *Hydrogen Storage Materials, Batteries, and Electrochemistry,* D. A. Corrigan and S. Srinivasan, Editors., PV 92-5, p. 141, The Electrochemical Society Proceedings Series, Pennington, NJ (1992).
5. T. Sakai, K. Muta, H. Miyamura, N. Kuriyama, and H. Ishikawa, *ibid.,* p. 59.
6. M. Viitanen, *This Journal,* **140,** 936 (1993).
7. Q. M. Yang, M. Ciureanu, D. H. Ryan, and J. O. Ström-Olsen, *ibid.,* **141,** 2111 (1994).
8. Q. M. Yang, M. Ciureanu, D. H. Ryan, and J. O. Ström-Olsen, *ibid.,* **141,** 2116 (1994).
9. B. E. Conway and J. Wojtowicz, *J. Electroanal. Chem.,* **326,** 277 (1992).
10. J. C. Slattery, *Momentum, Energy, and Mass Transfer in Continua,* 2nd ed., Robert E. Krieger Publishing Company, Huntington, New York (1981).
11. J. S. Newman, *Electrochemical Systems,* 2nd ed., Prentice Hall, Englewood Cliffs, NJ (1991).
12. Z. Mao, P. De Vidts, R. E. White, and J. S. Newman, *This Journal,* **141,** 54 (1994).

13. P. De Vidts and R. E. White, *ibid.*, **142,** 1509 (1995).
14. L. I. Antropov, *Theoretical Electrochemistry,* Mir Publishers, Moscow (1972).
15. H. Yayama, K. Hirakawa, and A. Tomokiyo, *Jpn. J. Appl. Phys.*, **25,** 739 (1986).
16. T. Sakai, H. Ishikawa, H. Miyamura, N. Kuriyama, S. Yamada, and T. Iwasaki, *This Journal,* **138,** 908 (1991).
17. R. M. Latanision and M. Kurkela, *Corrosion,* **39,** 174 (1983).
18. M. Ciureanu, D. H. Ryan, J. O. Ström-Olsen, and M. L. Trudeau, *This Journal,* **140,** 579 (1993).
19. J. J. G. Willems and K. H. J. Buschow, *J. Less-Common Met.*, **129,** 13 (1987).
20. H. Züchner, T. Rauf, and R. Hempelmann, *ibid.*, **172-174,** 611 (1991).
21. V. M. M. Lobo, *Handbook of Electrolyte Solutions,* Vol. A, Elsevier, New York (1989).
22. V. M. M. Lobo and J. L. Quaresma, *Electrolyte Solutions: Literature Data on Thermodynamic and Transport Properties,* Vol. II, Coimbra Editora Lda., Coimbra, Portugal (1981).
23. K. E. Brenan, S. L. Campbell, and L. R. Petzold, *Numerical Solution of Initial-Value Problems in Differential-Algebraic Equations,* North-Holland, New York (1989).
24. T. Sakai, H. Ishikawa, K. Oguro, C. Iwakura, and H. Yoneyama, *This Journal,* **134,** 558 (1987).

Electrochemical Impedance Spectroscopy Measurements on Lithium Salt Containing Interpenetrating Polymer Networks

Michael J. Hudson[a] and César A. C. Sequeira*[,b]

[a]*Department of Chemistry, University of Reading, Whiteknights, Reading RG6 2AD, England*
[b]*Department of Chemical Engineering, Instituto Superior Técnico, 1096 Lisbon Codex, Portugal*

ABSTRACT

The ionic conductivity of lithium interpenetrating polymer networks has been determined by electrochemical impedance spectroscopy. The effect of different amounts of lithium salt on the conductivity of these materials has been studied in the temperature range of 298 to 363 K. Conductivities of the order of 10^{-4} S cm^{-1} have been achieved. It was found that the conductivity was dependent on the amount of salt present in the interpenetrating polymer network and the maximum conductivity obtained was with a composition ratio of $(LiClO_4)$:$(PEO)_{88}$.

Introduction

Research and development in battery technology is extremely active in industry. One obvious reason for this is that the consumer is constantly interested in new battery systems which would perform a given function at a fraction of the cost of one it displaces. Better performance is another important driving force for research in this area. Higher energy density and/or rechargeable lithium batteries will find market acceptance if their performance is better than alternative systems.

At present, lithium battery systems offer the widest range of power sources for portable electronic and electrical equipment by virtue of their high energy density, long shelf life, and ability to work under extreme environmental conditions. The most recent research concerned with lithium battery technology has been the development of systems in which all of the components are solid.[1-9] This has posed the problem of developing a solid electrolyte, and work has been carried out on crystalline and amorphous electrolytes.

Crystalline electrolytes include compounds such as Li_3N, Na-beta alumina and many others.[10,11] This type of electrolyte, however, was difficult to prepare and was difficult to use. The complexity of preparing and working with such crystalline solid electrolytes therefore stimulated interest in amorphous electrolytes that were much easier to prepare and to work with. Polymers with high values of ionic conductivity were discovered as early as 1973, but it was not until 1978 that the dry polymer electrolyte concept was introduced, in the form of poly(ethylene oxide) (PEO) containing lithium perchlorate.[12-14] The type of PEO chosen was the high molecular mass linear variety which formed relatively strong, freestanding films at ambient temperature. Its strength was derived from a semicrystalline microstructure, in which stacked, chain-folded lamellar crystals were held together by long molecular chains extending from one crystal to the next via amorphous grain boundary regions. It was found that PEO formed direct interactions with Li^+ since the oxygen atoms in PEO contained free electron pairs which acted as donors for Li^+ when it was incorporated into a flexible chain. This ability of polyethers to act as polymer hosts is in part because of their flexibility which allows efficient cation coordination is illustrated in Fig. 1.

The amorphous, intergranular region of PEO was primarily responsible for the observed conductivity and not the crystalline phase. The conduction in such a polymer was thought to be due to the transfer of "sticky" ions from one chain to the next, in response to the continuous random twisting motion of the chains. Therefore, it was expected that, if the structure became increasingly ordered through crystallinity, then the chains would be held in a more regular structure and the conductivity would decrease, since the motion of the chains would be restricted. This presented a problem because PEO formed a high melting phase which was in equilibrium with pure crystalline PEO at low temperature (<57°C) or with an amorphous solution above the melting point of pristine PEO. Therefore, as expected, the conductivities of such single-phase $LiClO_4$:PEO systems were found to be sharply temperature dependent, varying from below 10^{-7} S cm^{-1} at room temperature to above 10^{-4} S cm^{-1} at the temperature required to melt most of the crystalline phase.

Figure 2 shows the conductivity of a typical single-phase $LiClO_4$:$(PEO)_8$ system, subjected to the following temperature cycle: (*i*) heat from 25 to 140°C at 10°C per min; (*ii*) hold at 140°C for 2 h; and (*iii*) cool from 140 to 70°C at 10°C per min, then cool from 70 to 25°C at 20°C per min. It is seen that the conductivity at room temperature was extremely low owing to the more regular, crystalline structure adopted by PEO under these conditions. However, on heating, the PEO passed through the crystalline melting point and an increase in conductivity was observed. This was the consequence of an increase in structural disorder in PEO which facilitated a more twisting motion of the long chains, and hence enhanced the transfer of ions from one chain

* Electrochemical Society Active Member.